minerals

MDPI

Article

Helium and Argon Isotopes in the Fe-Mn Polymetallic Crusts and Nodules from the South China Sea: Constraints on Their Genetic Sources and Origins

Yao Guan [1], Yingzhi Ren [2], Xiaoming Sun [1,2,3,*], Zhenglian Xiao [2] and Zhengxing Guo [2]

[1] School of Earth Sciences and Engineering, Sun Yat-sen University, Guangzhou 510275, China; guanyao@mail2.sysu.edu.cn

[2] School of Marine Sciences, Sun Yat-sen University, Guangzhou 510006, China; renyzh@mail2.sysu.edu.cn (Y.R.); xiaozhl3@mail2.sysu.edu.cn (Z.X.); guozhx7@mail2.sysu.edu.cn (Z.G.)

[3] Guangdong Provincial Key Laboratory of Marine Resources and Coastal Engineering, Guangzhou 510006, China

* Correspondence: eessxm@mail.sysu.edu.cn; Tel./Fax: +86-20-84110968

Received: 17 August 2018; Accepted: 8 October 2018; Published: 22 October 2018

check for updates

Abstract: In this study, the He and Ar isotope compositions were measured for the Fe-Mn polymetallic crusts and nodules from the South China Sea (SCS), using the high temperature bulk melting method and noble gases isotope mass spectrometry. The He and Ar of the SCS crusts/nodules exist mainly in the Fe-Mn mineral crystal lattice and terrigenous clastic mineral particles. The results show that the ^{3}He concentrations and R/R$_A$ values of the SCS crusts are generally higher than those of the SCS nodules, while ^{4}He and ^{40}Ar concentrations of the SCS crusts are lower than those of the SCS nodules. Comparison with the Pacific crusts and nodules, the SCS Fe-Mn crusts/nodules have lower ^{3}He concentrations and ^{3}He/^{4}He ratios (R/R$_A$, 0.19 to 1.08) than those of the Pacific Fe-Mn crusts/nodules, while the ^{40}Ar/^{36}Ar ratios of the SCS samples are significantly higher than those of the Pacific counterparts. The relatively low ^{3}He/^{4}He ratios and high ^{40}Ar concentrations in the SCS samples are likely caused by terrigenous detrital input with high radiogenic ^{4}He and ^{40}Ar contents. The SCS crusts and nodules have shorter growth periods, implying that in situ post-formation radiogenic ^{3}He, ^{4}He and ^{40}Ar produced by decay of U, Th and K have no effect on their isotope compositions. Thus, the SCS crusts/nodules inherited the noble gases characteristics of their sources. Helium and Ar isotope compositions in the SCS Fe-Mn crusts and nodules reflect the product of an equilibrium mixture between air-saturated seawater and radiogenic components during their growth, while the partial ^{3}He excess in some SCS samples may represent a little mantle-derived origin. The different He and Ar isotope compositions of the Fe-Mn crusts and nodules between the South China Sea and the Pacific Ocean are due to their different sources and genetic processes. The characteristics of He and Ar isotope compositions in the SCS polymetallic crusts and nodules are similar to the properties of hydrogenetic Fe-Mn oxide/hydroxide precipitates, which reflects mainly the product of an equilibrium mixture between air-saturated seawater and radiogenic components.

Keywords: Fe-Mn polymetallic crusts and nodules; helium and argon; isotope composition; genetic origin; South China Sea

1. Introduction

Noble gases are widely used in the studies of basic properties of geological systems and dynamics mechanism and have a unique advantage in marine science research. Because the different carrier phases of noble gases imported into the ocean have different isotopic compositions, noble gas isotopes provide important geological information for the research of modern ocean circulation, paleoceanography, seafloor hydrothermal and cold brine system and ocean/atmosphere gas exchange.

Early studies of marine noble gases are mainly concentrated in solving geochemical problems, such as tracing the excess He in the seawater, which is likely produced by U-Th series radioactive decay in the marine sediments [1,2]. After the discovery of mantle-originated helium [3] and ^{3}He originated near the sediment surface (via ^{3}H decay in the sea) [4], people began to use noble gases to trace the source of submarine hydrothermal fluids, crust/mantle material cycle, constrain the formation process and thermodynamic mechanism of seamount systems [5–11] and to explore the formation and cycle of the ocean currents (e.g., [12–14]).

Some studies have explored potential application of He isotopes in paleoceanography and these studies are built on the findings of extraterrestrial He in deep-sea sediments [15]. Merrihue [15] first recognized that the ^{3}He/^{4}He ratios of deep-sea sediments are about two orders of magnitude higher than that of the atmosphere and attributed that to the addition of the cosmic material. Systematic studies of He [16–23], Ne [24–27] and Ar [28–30] isotopes in the deep-sea sediments have also been conducted.

Widely distributed in the deep oceans, ferromanganese (Fe-Mn) crusts and nodules are important submarine mineral resources and contain abundant useful metals, such as Co, Ni, Cu, rare earth elements (REEs) and platinum group elements (PGEs) [31–37]. The Fe-Mn crusts and nodules also preserve long-term records of the chemical composition of seawater, which reveals changes in the delivery of material to the oceans and climate over tens of millions of years [38–40]. Helium and Ar are occurred in minerals as: (1) trapped in crystal gap or structural defects when mineral crystallized and occurred in mineral lattice or inclusions; (2) adsorbed on the mineral surfaces and occurred in the mineral surfaces and fractures; (3) produced by radioactive decay (e.g., of U, Th and K) and occurred in the mineral lattice or solid inclusions. After the mineral formation, the original nuclide contents and isotope compositions of the noble gases in the minerals could be changed by the accumulation of the radiogenic or cosmogenic noble gases and metasomatic fluid diffusion. Sano et al. [41] first studied the He and Ar isotopes of the deep-sea nodules from the Ogasawara Islands and Mariana Trough and suggested that extremely high ^{3}He/^{4}He ratios are caused by the input of extraterrestrial material. Subsequently, the He isotopes of the deep-sea nodules from the Pacific Clarion-Clipperton Fracture Zone (CCFZ) were studied [42–45]. These researches founded that the deep-sea nodules have high ^{3}He contents and ^{3}He/^{4}He ratios (5–54 R_A [42,45]) and that the sediments around the deep-sea nodules also have the high ^{3}He/^{4}He ratios [44]. Thus, these authors considered that the deep-sea nodules and sediments may have mixed with the interplanetary dust particles (IDPs) and mantle source [42–45]. Previous research on the noble gases compositions of the seamount Fe-Mn crusts from the Pacific Ocean yielded different ideas with respect to the sources of the noble gases [46–50]. Some studies suggested that He isotopes in the Fe-Mn crusts from the central and western Pacific Ocean are a mixture of cosmic He in extraterrestrial grains and radiogenic He in wind-borne dust [46,47,50]. Yet some studies indicated that the noble gases in the Fe-Mn crusts also from the central and western Pacific Ocean originate primarily from the mantle [48,49]. Shallow water Fe-Mn crusts and nodules occur in a number of places throughout the global ocean at water depths of <2000 m, these crusts and nodules accrete relatively rapidly and do not sequester large amounts of minor elements from seawater [37]. However, there are few systematic studies on the noble gases in shallow water Fe-Mn crusts and nodules. In this paper, we presented the He and Ar isotopes of the marginal-sea shallow water Fe-Mn polymetallic crusts/nodules from the South China Sea to determine the mixing sources of He and Ar components in the deposits with their geochemical environment of formation. Additionally, we collected the data of previous studies aimed at understanding the He and Ar isotope characteristics in the Fe-Mn crusts and nodules from the oceans in order to compare with each other.

2. Geological Setting

The South China Sea (SCS) is one of the largest marginal seas in the western Pacific and comprises a continental shelf, a continental slope and a central deep-sea basin, which the submarine topography is ladder-like from the continental margin to the center basin (Figure 1) [51]. The western and northern slope of the SCS is a passive continental margin, whereas the center is the deep-sea basin with dozens of seamounts. The complex submarine topography of the SCS, featured by its widely dispersed island reefs, platforms, plateaus, trough valleys and abyssal plain provides many locations for the growth of Fe-Mn nodules and crusts.

The SCS is located near the focus of the convergence between the Eurasian, Pacific-Philippine Sea and Indo-Australian plates along two regional convergent zones (the circum-Pacific and Tethyan zones) [52]. The South China Sea has developed faults in the diverse basement rocks, which mainly consist of Paleozoic to Mesozoic basement in the edge and Cenozoic metamorphic rocks in the center. Submarine volcanoes are widespread in the South China Sea (Figure 1) and mafic-intermediate volcanic activities were common from the Cretaceous to early Miocene (and continued locally after the early Miocene) [53–55]. The seismic tomography models clearly show a continuous low velocity channel originated from the mantle in the northern South China Sea, which is a tilted rising mantle plume [56].

The South China Sea is surrounded by numerous straits that communicate with the neighboring oceans. The northeastern South China Sea connects to the East China Sea and the northwestern Pacific Ocean through the Taiwan Strait and the Luzon Strait, respectively. The southeastern part connects with the Sulu Sea through the Mindulo Strait and the Barabak Strait and the southern part connects to the Java Sea through the Karimata Strait and Banga Strait. The southwestern part connects to the Indian Ocean through the Malacca Strait. The waters of the South China Sea mainly communicate with the Pacific Ocean through the Bashi Channel. In addition to the oceanic waters, the waters in the South China Sea are also obviously affected by the input of the surrounding terrestrial rivers. The main rivers flowing into the South China Sea are the Pearl River and the Red River in the north and the Mekong River and Chao Phraya River in the west. These rivers are the main source of the terrigenous materials in the South China Sea, of which the average water inflow to the South China Sea from the Pearl River over the years was 3.49×10^{11} m^3/year and the average sediment inflow carried was 8.3×10^7 t/year [57]. The total volume of sediments imported into the South China Sea since the Eocene is $7.01 \pm 1.48 \times 10^6$ km^3, the average deposition rate in the South China Sea is 62.2 m/Ma, which is much higher than that in the deep ocean (1 cm/ka [58]) and the average accumulation rate is 12.8 g/(cm^2·ka) [59].

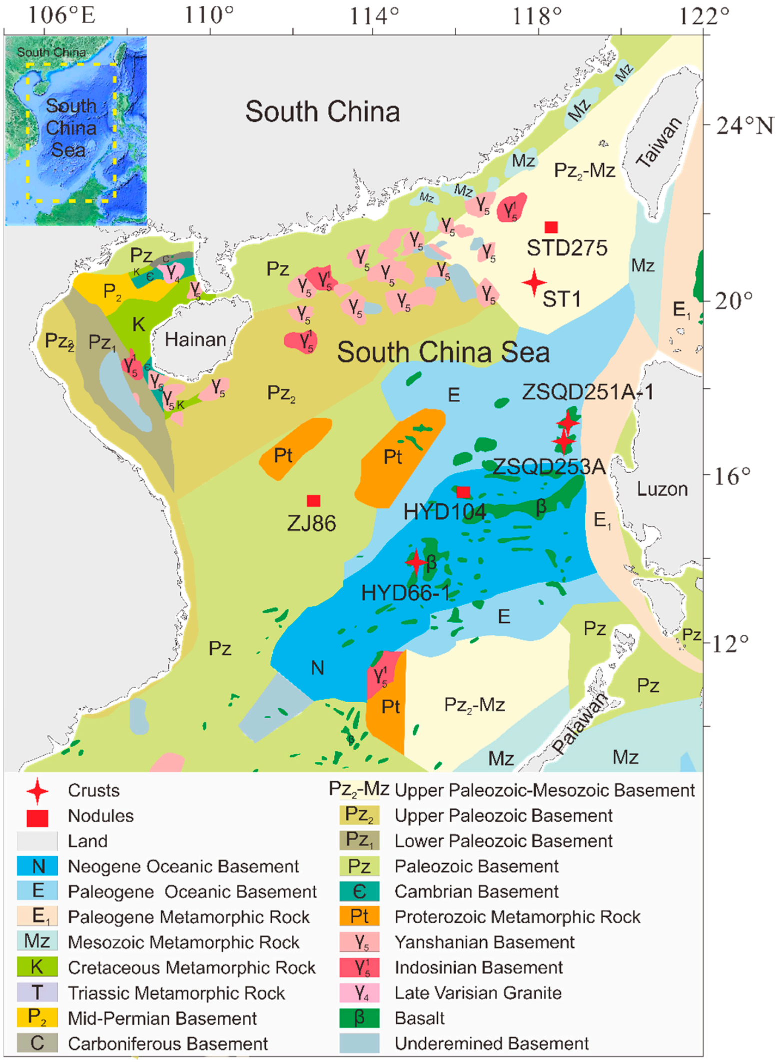

Figure 1. Map of the South China Sea basement and the sample locations (revised after Yang et al. [60]). Yellow dash-square on the top-left inset shows the location of the South China Sea.

3. Materials and Methods

3.1. Samples

The Fe-Mn crust/nodule samples investigated in this study were recovered from different sites in the South China Sea and were selected from dredge collected on the vessel "Haiyangsihao" during the SCS regional surveys. The range of sampling water depths is from 815 m to 2237 m (coordinates shown in Table 1). All samples analyzed were preserved in the sealed bags after dried, then placed in a drying cabinet. Samples ZJ86 were collected from the Zhongjian Islands, HYD66-1 and HYD104 from the Huangyan Islands, ST1 and STD275 from the northeastern SCS margin and ZSQD253A and ZSQD251A-1 were from the Zhongsha Islands (the sampling locations are shown in Figure 1). Samples ZJ86, STD275 and HYD104 are nodules, whereas samples HYD66-1, ST1, ZSQD253A and ZSQD251A-1 are crusts (Figure 2). More detailed morphological descriptions were given in Guan et al. [61].

Table 1. Sample descriptions and mineralogy of the Fe-Mn polymetallic crusts and nodules from the South China Sea.

Sample	Type	Sampling Location		Water Depth (m)	Nucleus or Substrate	XRD Mineral Compositions
ZJ86	Nodule	112°31.4679′ E	15°20.5275′ N	1945	Nucleus of clay containing some micro-nodules	δ–MnO_2, todorokite, buserite, goethite, feroxyhyte, quartz and plagioclase
STD275	Nodule	118°16.7459′ E	21°41.4902′ N	1548	Nucleus of dense rusty red iron oxide	δ–MnO_2, todorokite, goethite, feroxyhyte, quartz and plagioclase
HYD104	Nodule	116°10.9080′ E	15°33.8074′ N	815	Nucleus of biodetritus and some micro-nodules	δ–MnO_2, todorokite, buserite, goethite, quartz and plagioclase
ST1	Crust	117°54′37.5″ E 117°54′36.4″ E	20°28′26.7″ N 20°28′39.2″ N	1600	Substrate of altered basalt	δ–MnO_2, goethite, feroxyhyte, quartz, plagioclase and calcite
ZSQD251A-1	Crust	118°50.8666′ E	17°13.1088′ N	1950	Substrate of altered basalt	δ–MnO_2, goethite, quartz, plagioclase
ZSQD253A	Crust	118°36.3659′ E	16°45.9867′ N	1150	Substrate of reef limestone	δ–MnO_2, goethite, feroxyhyte, quartz, plagioclase and calcite
HYD66-1	Crust	115°16.3729′ E	13°40.7307′ N	1378	Substrate of amygdaloidal basalt	δ–MnO_2, todorokite, goethite, feroxyhyte, quartz and plagioclase

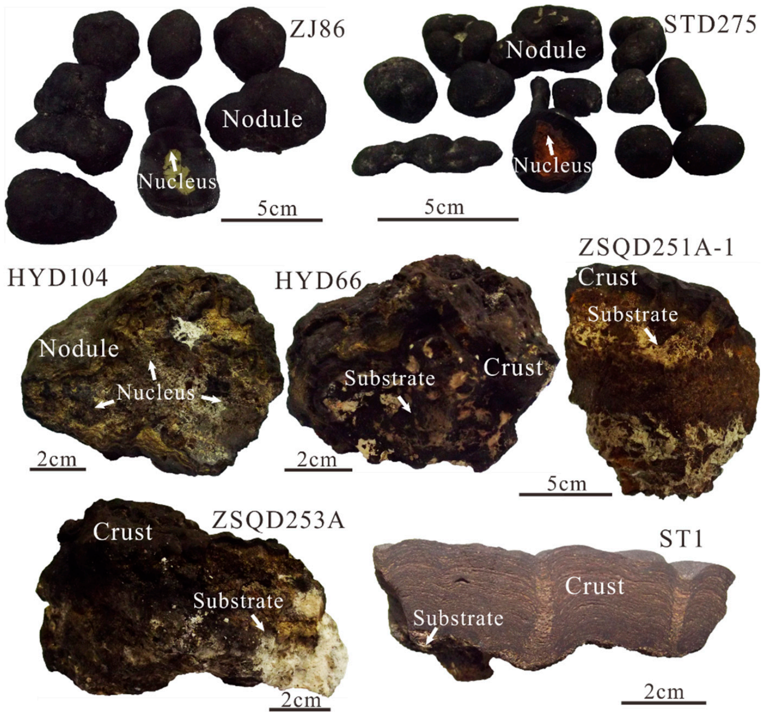

Figure 2. Sample photos of the SCS crusts and nodules analyzed.

The SCS nodules occurred in silty-clayey sediments and their nuclei include clay, silt and Fe oxides. The nodules show different morphological features, the nodule HYD104 shows conglomeratic and nodules STD275 and ZJ86 are ellipsoidal, spherical, polynucleate and irregular. The crusts show distinct laminated layers and accumulated onto rock substrates such as altered basalts, carbonate rocks and (bio)reef-limestone. The surfaces of the SCS crusts and nodules range from dark-brown to black and vary from being smooth to rough, warty or with cauliflower-like protrusions.

3.2. Mineralogy and Chemistry

X-ray powder diffraction (XRD) analysis was conducted at the State Key Laboratory for Mineral Deposits Research, Nanjing University. The results show that all samples have a composition typical of hydrogenetic precipitates with δ-MnO_2 and amorphous FeO(OH) as the main mineral phases. The samples also contain considerable amounts of quartz and plagioclase, as well as minor todorokite, buserite, goethite, feroxyhyte and calcite (Table 1).

The SCS samples were studied in detail with mineralogical, age, geochemical and isotopic analyses [61,62]. Analyses of major elements were analyzed using X-ray fluorescence spectrometer (XRF). Minor elements were determined by Inductively Coupled Plasma Atomic Emission Spectrometry (ICP-AES) and Inductively Coupled Plasma Mass Spectrometry (ICP-MS). The Mn/Fe ratios (less than 2.5) of the SCS samples analyzed are typical of hydrogenetic Fe-Mn precipitates [61], which are supported by the REY (REEs and yttrium) discrimination [63]. The growth rates of the SCS crusts and nodules were calculated using the empirical chronometer derived from formula where growth rate (GR) = $13.8 \times (Mn/Fe)^2 + 0.75$, with metals in wt.% [64]. This formula is considered a minimum age estimate and is not possible to exclude changes in growth rate within a bulk sample. The average growth rate of our samples analyzed is 21.54 mm/Ma [61]. The SCS polymetallic crusts and nodules were formed in epicontinental sea and have high growth rates and only the uppermost 1 cm of the nodules and crusts were analyzed to minimize the differences of the noble gases characteristics caused by the age differences.

3.3. Noble Gases Analysis

Helium and argon isotopes were analyzed on seven SCS polymetallic crusts and nodules. Noble gases nuclide concentration and their isotope compositions were determined at the Beijing Research Institute of Uranium Geology, China National Nuclear Corporation, using the Thermo Fisher Scientific (Waltham, MA, USA) Helix SFT noble gas mass spectrometer. The sample processing and testing processes were similar to those described in References [46,49], which include: (1) separate the Fe-Mn encrusts from their substrates or nuclei, then crush and sieve the samples. Collect the 40 to 60 mesh fraction, clean in acetone and then rinse in deionized water, in order to remove the secondary impurities; (2) after drying, weight and place the samples into aluminum foil packets; (3) the samples were step heated at 130 °C for 24 h to drive off the surface adsorbed gases, then melted at 1600 °C in a double-vacuum furnace of an ultra-high vacuum pressure system; (4) purify the mixed gases (which contain the He and Ar released by liquation) by removing the contained reactive gases via exposure under a hot Zr-Al pump, then the Ar is equilibrated with the liquid nitrogen-cooled activated charcoal finger. Helium content and isotope compositions are measured by the isotope mass spectrometer; (5) after measuring the He isotope compositions, remove the liquid nitrogen-cooled charcoal finger and heated. Argon content and isotope compositions were determined using the mass spectrometer.

The instrument blank background of ^{40}Ar is below 1.0×10^{-15} mol at room temperature and below 1.0×10^{-14} mol at 1300 °C. The faraday cup of instrument resolution is over 400 and ion multiplier is over 700; the sensitivity is better than that of 2×10^{-4} A/Torr when He is in the 800 µA of trap current, while the sensitivity is better than that of 7×10^{-4} A/Torr when Ar is in the 200 µA of trap current. The measurements were normalized to the measurement standards of atmospheric He and Ar isotope compositions, which the ratio of ^{3}He and ^{4}He is $(1.399 \pm 0.013) \times 10^{-6}$, the ratio of ^{40}Ar and ^{36}Ar is 295.6 and that of ^{38}Ar and ^{36}Ar is 0.187. The isotopic data are reported where the analytical error is below 10%.

4. Results

4.1. Helium and Ar Isotope Compositions of the SCS Crusts and Nodules

The He and Ar isotope compositions and the related parameters of the SCS crusts and nodules are listed in Table 2. The ^{3}He concentrations and R/R_A values of the SCS crusts are generally higher than those of the SCS nodules, while ^{4}He and ^{40}Ar concentrations of the SCS crusts are lower than those of the SCS nodules. The ^{4}He contents ($cm^3 \cdot STP \cdot g^{-1}$, same below) of the SCS crusts analyzed range from 0.37×10^{-7} to 2.58×10^{-7} (average 1.03×10^{-7}) and ^{3}He contents range from 3.48×10^{-14} to 10.91×10^{-14} (average 7.16×10^{-14}). The ^{3}He/^{4}He ratios of the SCS crusts range from $4.23 \pm 0.14 \times 10^{-7}$ to $15.10 \pm 0.28 \times 10^{-7}$ (average $9.17 \pm 0.25 \times 10^{-7}$) and their atmosphere-normalized values (R/R_A) range from 0.30 ± 0.01 to 1.09 ± 0.02 (average 0.65 ± 0.02). The ^{40}Ar of the SCS crusts and nodules range from 0.18×10^{-6} to 0.84×10^{-6} (average 0.49×10^{-6}) and the ^{40}Ar/^{36}Ar ratios range from 467.6 ± 0.65 to 873.9 ± 1.01 (average 688.3 ± 0.82).

Table 2. Helium and Ar isotope compositions ($cm^3 \cdot STP \cdot g^{-1}$) and ratios of the Fe-Mn crusts and nodules from this study and other literatures.

Type	Sample	Description	Region	^4He ($\times 10^{-7}$)	^3He ($\times 10^{-14}$)	$^3He/^4He$ ($\times 10^{-7}$)	R/R_A ($\pm 1\sigma$)	^{40}Ar ($\times 10^{-6}$)	$^{40}Ar/^{36}Ar$ ($\pm 1\sigma$)	$^{40}Ar^*$ ($\times 10^{-7}$)	$^{40}Ar^*$ (%)	$^{40}Ar^*/^4He$
Shallow-water Fe-Mn nodules	ZJ86	axiolitic	the South China Sea (this stduy)	1.33	4.68	3.52 ± 0.14	0.25 ± 0.01	0.79	664.0 ± 0.96	4.39	55.5	3.3
	STD275	globular		3.61	9.64	2.67 ± 0.28	0.19 ± 0.02	1.04	588.4 ± 0.66	5.17	49.78	1.43
	HYD104	psephitic		0.31	2.68	8.65 ± 0.28	0.62 ± 0.02	1.5	329.0 ± 0.39	1.52	10.18	4.89
Shallow-water Fe-Mn crusts	ST1	platy		2.58	10.91	4.23 ± 0.14	0.30 ± 0.01	0.84	873.9 ± 1.01	5.55	66.19	2.15
	HYD66-1	platy		0.69	10.36	15.10 ± 0.28	1.09 ± 0.02	0.56	664.8 ± 0.82	3.11	55.55	4.53
	ZSQD253A	strumae		0.49	3.89	7.94 ± 0.28	0.57 ± 0.02	0.39	467.6 ± 0.65	1.44	36.81	2.95
	ZSQD251A-1	platy		0.37	3.48	9.41 ± 0.28	0.67 ± 0.02	0.18	746.8 ± 0.78	1.06	60.43	2.84
Shallow-water Fe-Mn nodules	1		the Baltic Sea [65]	137	130	0.95	0.07					
	2			164	130	0.82	0.06					
	3			117	450	3.80	0.27					
	4			130	130	1.00	0.07					
	5			156	137	0.88	0.06					
Oceanic crusts	CL01	Low $^3He/^4He$ crusts	the central and western Pacific Ocean [48]	4.21		31.40	2.25	10.98	457.0			
	CX07			0.43		40.90	2.92	0.77	543.0			
	MD53			2.16		39.00	2.79	6.97	447.0			
	MH68			0.85		28.50	2.04	1.60	481.0			
	MP2-09	High $^3He/^4He$ crusts		0.10		145.0	10.30	5.78	298.0			
	MP3-20			0.08		168.0	12.0	5.35	293.0			
	MP5-17			0.17		146.0	10.40	9.05	299.0			
	CA06	Bulk	Pacific Magellan seamounts [49]	0.75			8.89	1.39	355.6			
	CA09			0.18			4.60	5.85	305.1			
	M18D110			0.45			5.69	4.43	299.2			
	M19D111	Outer encrusts		1.13			4.64	65.41	298.0			
	M19D112	Intermediate encrusts		0.90			15.600	17.47	290.3			
	M19D113	Inner crusts		1.64			5.49	78.40	296.0			
	M19D121	Substrate rock		5.06			1.56	7.97	311.9			
	MHD79-I	Profile (from old to new)	The central Pacific MH seamount [50]		0.06	260.8	18.63		263.9			
	II				0.02	121.7	8.69		249.8			
	III				0.05	135.2	9.66		295.5			
	IV				0.03	4299	307.1		291.4			
	V				0.03	3149	224.9		292.2			
	VI				0.15	51121	3651		270.4			
	VII				0.03	7041	503.0		288.7			

Table 2. *Cont.*

Type	Sample	Description	Region	^{4}He ($\times 10^{-7}$)	^{3}He ($\times 10^{-14}$)	^{3}He/^{4}He ($\times 10^{-7}$)	R/R$_A$ ($\pm 1\sigma$)	^{40}Ar ($\times 10^{-6}$)	^{40}Ar/^{36}Ar ($\pm 1\sigma$)	^{40}Ar* ($\times 10^{-7}$)	^{40}Ar* (%)	^{40}Ar*/^{4}He
Oceanic crusts	0303W	Outer encrusts	the western Pacific Ocean [47]	0.85		26.58	1.90	8.11	345	11.63	14.35	
	0303S	Porous encrusts		0.77		394.5	28.20	5.47	310.1	2.57	4.71	
	0303L	Compact encruts (Phosphatization)		15.59		0.77	0.06	12.77	305.1	4.02	3.15	
	0321W	Outer encrusts		0.20		31.34	2.24	0.858	349.5	1.33	15.45	
	0321S	Porous encrusts		0.95		134.0	9.58	18.08	300.9	3.24	1.79	
	0321L	Compact encrusts (Phosphatization)		1.63		60.3	4.31	1.07	349.5	1.65	15.45	
	0346W	Outer encrust		0.23		40.01	2.86	1.43	324.6	1.28	8.97	
	0346S	Porous encrusts		0.20		85.48	6.11	13.24	302	2.85	2.15	
	0346L	Compact encruts (Phosphatization)		4.08		0.49	0.04	78.62	299.2	9.72	1.24	
	VA13/2(0-1)a		the central Pacific Ocean [46]				237.7					
	VA13/2(0-1)b						1852					
	VA13/2(0-1)c						312					
	VA13/2(0-1)d						983					
	VA13/2(1-2)						106					
	VA13/2(2-3)						84					
	VA13/2(3-4)						110.6					
	VA13/2(4-5)						66.7					
	VA13/2(5-6)a						297.5					
	VA13/2(5-6)b						26.2					
	VA13/2(5-6)c						29.6					
	VA13/2(5-6)d						32.6					
	VA13/2(6-7)						251.8					
	VA13/2(7-8)						159.6					
	VA13/2(8-9)						240					
	VA13/2(9-10)						18.5					
	CD29-2(4-5)						14.9					
	CD29-2(10-11)						14.6					
	CD29-2(12-13)						23.9					
	CD29-2(15-16)						17.9					
	CD29-2(17-18)						9.2					
	CD29-2(19-20)						8.3					
	CD29-2(21-22)						8.4					

Table 2. *Cont.*

Type	Sample	Description	Region	^{4}He ($\times10^{-7}$)	^{3}He ($\times10^{-14}$)	^{3}He/^{4}He ($\times10^{-7}$)	R/R$_A$ ($\pm1\sigma$)	^{40}Ar ($\times10^{-6}$)	^{40}Ar/^{36}Ar ($\pm1\sigma$)	^{40}Ar* ($\times10^{-7}$)	^{40}Ar* (%)	^{40}Ar*/^{4}He
Oceanic crusts	CD29-2(23-24)		the central Pacific Ocean [46]				9.7					
	CD29-2(25-26)						4					
	CD29-2(27-28)						10.3					
	CD29-2(29-30)						5.3					
	CD29-2(31-32)						7.5					
	CD29-2(43-44)						6.2					
	CD29-2(45-46)						1.4					
	CD29-2(47-48)						2.9					
	CD29-2(49-50)						0.87					
	CD29-2(51-52)						0.21					
	CD29-2(53-54)	Phosphatization					0.18					
	CD29-2(55-56)	Phosphatization					0.14					
	CD29-2(57-58)	Phosphatization					0.064					
	CD29-2(61-62)	Phosphatization					0.038					
	CD29-2(67-68)	Phosphatization					0.12					
	CD29-2(71-72)	Phosphatization					0.15					
	CD29-2(18-19B)						0.033					
	CD29-2(16-17B)						0.062					
	CD29-2(14-15B)						0.046					
	CD29-2(12-13B)											
	CD29-2(10-11B)						0.034					
	CD29-2(6-7B)						3.4					
	CD29-2(2-3B)											
	CD29-2(0-1B)											
Oceanic nodules	KH-84-1-16-001		Mariana Trough [41]	1300		44	3.15	1.2	835			
	KH-84-1-19-A			1300		151	10.79	1.2	807			
	KH-84-1-19-B			940		43	3.07	1	316			
	KH-84-1-19-C							1.5	333			
	KH-84-1-25			490		225	16.08	1.2	324			
	KH-84-1-2-124		Ogasawara region [41]	260		15	1.07	1.1	311			
	KH-84-1-3-606			98		593	42.39	2.6	384			
	KH-84-1-3-607			580		59	4.22		290			
	KH-84-1-5-33			1200		102	7.29	4.7	313			
	KH-84-1-27-017			120		60	4.29	2.3	432			
	ND06	Cauliflower-like	Pacific CCFZ nodules [33]	1.52	709.5	466.8	33.34	24.9	298.6			
	ND105-4	Cauliflower-like		0.93	370.8	399.1	28.51	21.8	299			
	ND05	Living body-like		30.5	554.2	18.17	1.298	15.1	308.4			
	ND02	Living body-like		1.14	474.9	417.3	29.81	17.1	300.4			
	ND105-8	Cauliflower-like		1.25	371.0	296.1	21.15	12.71	307.8			
	ND105-0	Cauliflower-like		1.03	848.1	821.8	58.7	16.2	301.3			

Table 2. *Cont.*

Type	Sample	Description	Region	^{4}He ($\times10^{-7}$)	^{3}He ($\times10^{-14}$)	^{3}He/^{4}He ($\times10^{-7}$)	R/R$_A$ ($\pm1\sigma$)	^{40}Ar ($\times10^{-6}$)	^{40}Ar/^{36}Ar ($\pm1\sigma$)	^{40}Ar* ($\times10^{-7}$)	^{40}Ar* (%)	^{40}Ar*/^{4}He
Oceanic nodules	8251		Pacific CCFZ nodules [45]	21.17	1620	76.53	5.47					
	8202			3.55	744	209.9	15					
	8096			3.01	649	215.5	15.4					
	8001			0.71	239	338.6	24.2					
	5234		Pacific CCFZ nodules [43]	2.02	349	173	12.37					
	5234			1.55	2055	1326	94.78					
	5420			2.44	566	232	16.58					
	5420			3.24	3366	1039	74.27					
	5314			3.1	1082	349	24.95					
	5314			1.63	1214	745	53.25					
	5302			1.73	907	524	37.46					
	5302			1.34	596	445	31.81					
	5459			1.82	803	441	31.52					
	5459			1.75	1005	574	41.03					
	1			1.92	1448	754	53.90					
	1			2.17	846	390	27.88					
	2			1.98	786	397	28.38					
	2			1.72	351	183	13.08					
	3			1.27	352	277	19.80					
	3			3.21	607	189	13.51					
	4			5.28	1030	195	13.94					
	5			3.4	357	105	7.51					

R = ^{3}He/^{4}He ratio of the sample; R$_A$ = Atmospheric ^{3}He/^{4}He ratio (1.399 × 10^{-6} [58]); ^{40}Ar* = (^{40}Ar)$_{sample}$ × (1 − (^{40}Ar/^{36}Ar)$_{air}$/(^{40}Ar/^{36}Ar); ^{40}Ar* % = ((^{40}Ar/^{36}Ar)$_{sample}$ − 295.5)/(^{40}Ar/^{36}Ar)$_{sample}$ × 100.

The ^{4}He contents of the SCS nodules analyzed range from 0.31 × 10^{-7} to 3.61 × 10^{-7} (average 1.75 × 10^{-7}) and ^{3}He contents range from 2.68 × 10^{-14} to 9.64 × 10^{-14} (average 5.67 × 10^{-14}). The ^{3}He/^{4}He ratios of the SCS crusts range from 2.67 ± 0.28 × 10^{-7} to 8.65 ± 0.28 × 10^{-7} (average 4.95 ± 0.23 × 10^{-7}) and their R/R_A range from 0.19 ± 0.02 to 0.62 ± 0.02 (average 0.35 ± 0.02). The ^{40}Ar of the SCS crusts and nodules range from 0.79 × 10^{-6} to 1.50 × 10^{-6} (average 1.11 × 10^{-6}) and the ^{40}Ar/^{36}Ar ratios range from 329.0 ± 0.39 to 664.0 ± 0.96 (average 527.1 ± 0.67).

4.2. Spatial Differences of He and Ar in the SCS Crusts and Nodules

The crust ST1 from the northern SCS margin has the highest ^{4}He (2.58 × 10^{-7}) and ^{3}He (10.91 × 10^{-14}) contents among all the SCS crust samples. The crusts ZSQD253A and ZSQD251A-1 from the Zhongsha Islands have lower ^{4}He, ^{3}He and ^{40}Ar contents than the other SCS crusts. The nodule STD275 from the same area as the crust ST1 has higher ^{4}He (3.61 × 10^{-7}) and ^{3}He (9.64 × 10^{-14}) contents than the other SCS nodules. In addition, the crust HYD66-1 and the nodule HYD104, both from near the Huangyan Islands, have the highest ^{3}He/^{4}He ratios (15.10 × 10^{-7} and 8.65 × 10^{-7}, respectively) among the SCS crusts and nodules analyzed.

5. Discussion

5.1. Comparison of the He and Ar Isotope Characteristics with Deep-Sea Samples

For comparison, the Table 2 also shows the data of the Fe-Mn crusts and nodules from the Pacific Ocean and the Baltic Sea, respectively, The He and Ar of the SCS Fe-Mn crusts/nodules are different from those of the Fe-Mn crusts [46,47,49] and nodules [33,41,65] from the other regions, respectively. Generally, the ^{4}He contents of the SCS crusts are similar to those of the Pacific non-phosphatized crusts. But the R/R_A values of the SCS crusts are significantly lower than those of the Pacific crusts [46–50], while similar to those of the Pacific phosphatized crusts [46,47]. This may be likely that the high ^{4}He concentration in the Pacific phosphatized crusts reflects better retention of radiogenic helium resulted from phosphatization [46]. In addition, the ^{40}Ar contents of the SCS crusts are lower than those of the Pacific crusts but the ^{40}Ar/^{36}Ar of the former are much higher than those of the later [47–50].

^{4}He contents of the SCS nodules are similar to those of the Pacific CCFZ nodules [33,43,45] but lower than those of the nodules from Mariana Trough and Ogasawara region [41]. The R/R_A values of the SCS nodules are also obviously lower than those of the nodules from the Pacific Ocean [33,41,43,45]. The ^{40}Ar concentrations of the SCS nodules are lower than those of the Pacific CCFZ nodules but similar to nodules from the Mariana Trough and Ogasawara region [41]. As the shallow-water nodules, ^{4}He and ^{3}He concentrations of the SCS nodules are significantly lower than those of the nodules from the Baltic Sea, while the R/R_A values of the former are higher than the later [65]. These characteristics suggest significant noble gases source differences (of the Fe-Mn crusts/nodules) between the South China Sea and the other regions.

5.2. Forms of He and Ar Occurrence in the SCS Crusts and Nodules

The SCS polymetallic crusts and nodules were deposited on over 800 m deep-seafloor. In this study, we adopted the high-temperature melting method to analyze the noble gases compositions, thus minimizing adsorbed noble gases (on mineral surface). Terrigenous dust/clastics formed by continental erosion were carried into the ocean by wind and rivers and their influence on crust/nodule chemical and mineral compositions are stronger for those formed in the marginal sea environment (e.g., SCS). Silica is enriched relative to Al in the continental margin crusts and nodules compared to open-ocean crusts and nodules [37,61]. Bulk rock Si contents of the SCS crusts and nodules analyzed range from 7.03% to 18.45% [61], while bulk rock Si contents of the Pacific Prime Zone crusts and Peru Basin nodules are 4.05% and 4.82%, respectively [37]. This indicates that there is a mass of terrigenous dust/clastics in the SCS crusts and nodules. The high contents of radiogenic He in the terrigenous dust/clastics (R/R_A: ~0.05) would influence the ^{3}He/^{4}He ratios and He concentrations of the SCS crusts and nodules. Therefore, the carrier phases of He and Ar in the SCS crusts/nodules are mainly the Fe-Mn mineral crystal and terrigenous clastic mineral particles.

5.3. Sources of He and Ar in the SCS Crusts and Nodules

The He and Ar concentrations and their isotope compositions can be changed by the accumulation of radiogenic ^4He and ^{40}Ar, which is controlled mainly by the U, Th and K contents and the formation time. Nucleogenic ^3He can be generated via the reaction on ^6Li (n, α) ^3H (β) ^3He, where the neutrons originate from (α, n) reactions on light elements [46]. The nucleogenic ^3He can change the He isotope composition of the system. The empirical formula method has yielded an average growth rate of 21.54 mm/Ma for the SCS crusts/nodules, which is much higher than that of most of hydrogenetic Fe-Mn crusts and nodules (1–5 mm/Ma [37]). The SCS Fe-Mn polymetallic crusts/nodules grow much faster than those formed in open oceans, thus their ore-forming periods are relatively short [61]. The radioactive half-lives of ^{40}K, ^{238}U, ^{235}U and ^{232}Th producing in situ ^4He and ^{40}Ar are 1250 Ma [66], 4,470 Ma, 704 Ma and 14,050 Ma [67] and the α particles which the ^6Li radioactive decay required come from the decay reaction of U and Th [68]. The influence of ^3He which is produced by radioactive genetic ^4He, ^{40}Ar and nuclear reactions on the noble gases isotope compositions of the SCS crusts and nodules is very limited, implying that in situ post-formation radiogenic ^3He, ^4He and ^{40}Ar produced are not quantitatively retained by the minerals [46]. Thus, the SCS crusts/nodules inherited the noble gases characteristics of their sources. It is pertinent here to discuss the main possible sources of He and Ar in the SCS Fe-Mn crusts and nodules.

5.3.1. Extraterrestrial Source

Previous studies on deep-sea sediments [15–19] and nodules [41,43,44] and seamount crusts [46,47,50,69] in the open oceans suggested that the extremely high $^3He/^4He$ ratio reflects extraterrestrial inputs, such as IDPs. Helium isotope characteristics of individual IDPs collected in the stratosphere were analyzed, yielded $^3He/^4He$ ratios of mainly 2.4×10^{-4} (172R_A) and the ^3He content of 1.9×10^{-5} $cm^3 \cdot STP \cdot g^{-1}$ [70]. Nevertheless, the IDP $^3He/^4He$ ratios can be up to 2221 ± 68 R_A [71] and those of meteorite particles can be up to 1543 ± 357 R_A [72]. Therefore, the ^3He contents of IDPs are approximately eight orders of magnitude higher than those of terrigenous materials and even mixing small amounts of extraterrestrial materials into deep-sea sediments can affect the $^3He/^4He$ ratios and ^3He contents of the latter. The 1 cm thickness Fe-Mn encrusts using the average growth rate of 21.54 mm/Ma should cover the growth period of 0.46 Ma. Takayanagi and Ozima [17] estimated the relatively constant flux of ^3He extraterrestrial input (in the past 40 Myr) to be $(1.5 \pm 1.0) \times 10^{-12}$ $cm^3 \cdot STP \cdot g^{-1} \cdot Ka^{-1}$. If the SCS samples incorporated some amount of IDPs over 0.46 Ma, their ^3He concentration should accumulate to $(6.9 \pm 4.6) \times 10^{-10}$ $cm^3 \cdot STP \cdot g^{-1}$. However, the ^3He concentrations of the SCS crusts and nodules (2.65×10^{-14} to 10.91×10^{-14} $cm^3 \cdot STP \cdot g^{-1}$) are about four orders of magnitude lower than estimated value and nine orders of magnitude lower than those of typical IDPs. This suggests that significant extraterrestrial-derived He contributions to the SCS crusts/nodules were unlikely.

5.3.2. Crustal Source

The He isotope compositions of the SCS crusts and nodules are among the field of the crustal, atmospheric and the mantle He. Therefore, He was trapped during formation of the SCS Fe-Mn crusts and nodules reflecting likely the mixture between radiogenic crustal, air-saturated seawater and/or mantle-derived He during their growth. In addition, in the $^{40}Ar/^{36}Ar$ versus R/R_A diagram (Figure 3), the SCS crusts/nodules are also plotted in the field between the crustal and mantle sources and the data points trend towards the atmospheric saturated seawater.

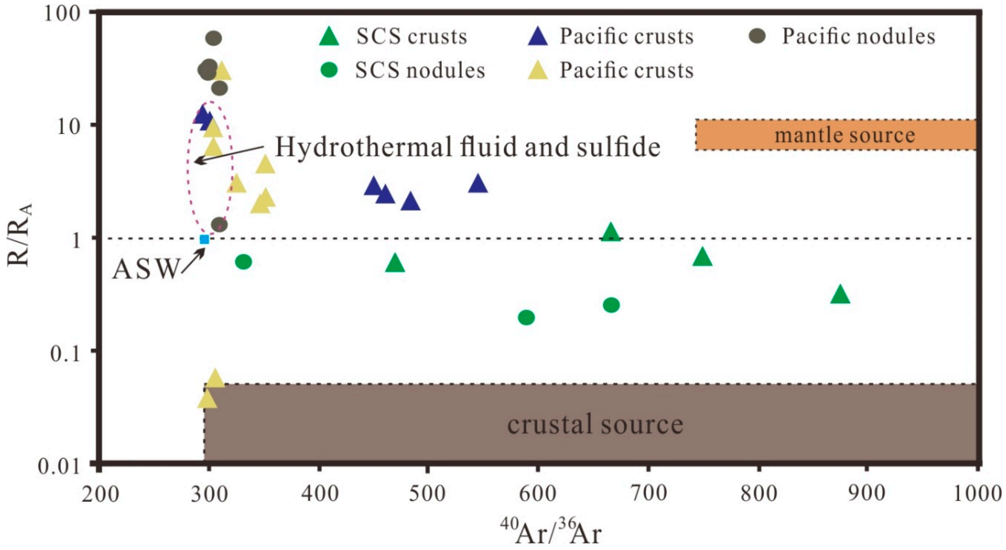

Figure 3. $^{40}Ar/^{36}Ar$ vs. R/R_A diagram of the SCS Fe-Mn crusts and nodules (revised after Burnard et al. [73]; green triangles and circles of SCS crusts and nodules data from this study; grey circles of Pacific nodules data from [33]; yellow and blue triangles of Pacific crusts data from [47,48], respectively).

The SCS crusts/nodules contain abundant terrigenous detrital quartz and feldspar compared to the Pacific Fe-Mn crusts/nodules [37,62]. The ^4He contents of the SCS crusts range from 0.37×10^{-7} to 3.61×10^{-7} $cm^3 \cdot STP \cdot g^{-1}$, which are similar to the Pacific non-phosphatized crusts (Table 2) [47–49]. The ^4He contents of the SCS crusts are not very different from their Pacific counterparts. ^4He contents of the SCS nodules are much lower than those of the nodules from the Mariana Trough, Ogasawara region [41] and the Baltic sea [65], while are similar to the Pacific CCFZ nodules. The relatively low $^3He/^4He$ ratios in the SCS samples are likely caused by terrigenous detrital input with high radiogenic ^4He contents. This suggests that the radiogenic ^4He in the terrigenous detrital minerals influence on the He of the SCS sample set will be significant.

Furthermore, ^4He concentrations of the nodules are much higher than those of the crusts (Table 2). According to the principle of mass conservation, Suess and Wanke [1] speculated that U and Th in the pelagic sediments would decay to produce ^4He-rich sediment pore-water and there would be significant radioactive ^4He flux from the deep-sea sediments into the ambient seawater [74]. The nodules are directly grown or buried under the surface of sediments, whose ^4He may be influenced by the combined effects of terrestrial substances and the ^4He-rich sediment pore-water, which are featured by their high ^4He abundances. Thus, the nodules have higher ^4He concentration than the crusts.

5.3.3. Atmospheric/Seawater Source

Solubility of noble gases in seawater increases with increasing atomic weight, thus the solubility of He is the lowest (e.g., He content in Pacific deep seawater: 1.2×10^{-12} $atoms \cdot g^{-1}$ [75]). This is because the varying concentrations of noble gases are controlled by their respective solubility equilibrated with the air [76]. The ^4He concentration in the air (and hence in atmospheric saturated water) at 20 °C is 4.6×10^{-8} $cc \cdot STP \cdot g^{-1}$ [77] but helium will be some 20% less soluble in seawater than in fresh water due to the salting out effect [75,78]. The $^3He/^4He$ ratios of the SCS crusts/nodules (except HYD66-1) range from 0.25 to 0.67 R_A where the He in these samples represents a mixture between radiogenic crustal He (0.01–0.05 R_A) and air-saturated seawater (<1 R_A). Although atmospheric He contribution to deep-sea sediments may be negligible [19,74], the He trapped in the Fe-Mn crusts and nodules cannot be neglected because the Mn-Fe oxide/hydroxide colloid are formed directly in the ambient seawater. However, Ar is more soluble in seawater than He, hence seawater has the same Ar isotope compositions as the atmosphere and deep-sea sediments often inherit the Ar isotopes of seawater [47]. Figure 3 shows that the SCS crusts/nodules contain seawater-like Ar isotope compositions. Radiogenic ^{40}Ar* contents in geological samples can be determined by the following equation [79]:

$$^{40}\text{Ar*}(\%) = ((^{40}\text{Ar}/^{36}\text{Ar})_{\text{sample}} - 295.5)/(^{40}\text{Ar}/^{36}\text{Ar})_{\text{sample}} \times 100 \quad (1)$$

The results show that the SCS crust/nodule ^{40}Ar* contents are of 10.18 to 66.19% (average 44.78%), indicating that there were partial seawater-derived ^{40}Ar contributions. Therefore, the Ar sources of the SCS crusts/nodules include mainly seawater and radiogenic components.

5.3.4. Mantle Source

The ^{3}He/^{4}He ratios of the SCS crust HYD66-1 is 1.08 R_A and the ^{3}He concentrations of the SCS sample HYD66-1, ST1 and STD275 range from 9.64×10^{-14} to 10.91×10^{-14} (cm^3·STP·g^{-1}), which are distinctly higher than those of the radiogenic crust and air-saturated seawater. The isotopic ratio of helium dissolved in seawater gradually increase with water depth in the Pacific and adjacent seas of Southwest Japan, which contains excess ^{3}He in the deep water derived from the mantle source [5,8,76,77,80–83]. This reflects that the excess ^{3}He in the SCS sample HYD66-1, ST1 and STD275 may have trapped the He released into seawater by the mantle degassing from the underlying seamounts and/or seawater-rock alteration of submarine basalt. In the mantle, noble gases and volatiles are commonly trapped in the mantle minerals, such as pyroxene, olivine and basaltic glass. If there is no mantle-derived magmatic activity, it would be difficult for the noble gases to diffuse to the seafloor [84]. The mantle He mainly inputs to seawater through volcanic activity [85] and through hydrothermal fluid upwelling associated with regional/local tectonic activity [86,87]. In addition, the weathering of seamount also provides materials for the formation of Fe-Mn crusts. The emplacement of the seamounts may have provided a channel of mantle degassing into seawater for the excess ^{3}He with mantle-derived characteristics [7], which may have trapped by the Fe-Mn oxide/hydroxide colloids formed in the ambient seawater. Thus, the excess ^{3}He in the crust HYD66-1 may represent minor mantle-derived origin.

5.4. Petrogenetic Significance for the SCS Crusts and Nodules

The He isotope compositions of the marine Fe-Mn crusts can be significantly altered by phosphatization [46,47]. Basu et al. [46] shows that the ^{3}He/^{4}He ratios of the Pacific seamount phosphatized crusts are significantly different from those of the non–phosphatized crusts and the former shows relatively low ^{3}He/^{4}He ratio similar to the SCS crusts and nodules. Sun et al. [47] analyzed the He and Ar isotope compositions of the seamount crusts and the phosphate substrate rocks formed by phosphatization from the Pacific Ocean, which showed the characteristics of high ^{4}He abundance and low ^{3}He/^{4}He ratio (0.087 R_A) and the Ar isotope compositions of the phosphatized crusts did not change significantly relative to that of the non–phosphatized crusts. For the oceanic seamount crusts, the old layers of the crusts are often seen as the effect of phosphatization. This reflects that large number of ^{4}He-rich fluorocarbon apatite (CFA) may have directly filled in the pores of the crusts or replaced the original calcareous microfossils [34,46], yet the phosphatization did not significantly alter the ^{3}He contents of the crusts [50]. Therefore, the effect of phosphatization on the He and Ar compositions in the seamount crusts just changes their ^{4}He abundances, while ^{40}Ar abundances do not alter significantly. The SCS crusts and nodules are not affected by the effect of the phosphatization and hydrothermal process during their growth processes [61,62], the He and Ar isotope features of the SCS crusts/nodules were more likely the effect of their material sources.

The mineral composition, metallogenic elemental geochemistry and genetic mechanism of the oceanic Fe-Mn crusts and nodules have been studied in detail [31,34–37,88–93]. The genetic types of Fe-Mn crusts and nodules are traditionally distinguished using the ternary Mn-Fe-10(Cu + Co + Ni) discrimination diagram [94] and this method has been widely used. Essentially discrimination diagrams that are also in use for marine Fe-Mn oxide/hydroxide precipitates are based on the REY signature [63]. Fe-Mn crusts precipitate directly from low-temperature ambient seawater (hydrogenetic) onto rock substrates. Fe-Mn nodules form by hydrogenetic and diagenetic precipitation on the surface of sediment. Diagenetic precipitation occurs from sediment pore fluids that consist of seawater modified by chemical reaction within the sediment column. Hydrothermal manganese and iron deposits occur near hydrothermal field [37]. Thus, these classifications are in three main categories: hydrogenetic, diagenetic and hydrothermal. The terminology is based on where the type of aqueous fluid from which the Fe-Mn oxides/hydroxides precipitate [63]. Noble gases provide new information for the studies of the material source and genesis of Fe-Mn crusts and nodules, because the noble gas isotope signature is well known for their different sources in natural environments. The He and Ar isotope composition of each type of aqueous fluid has distinct characteristics. Hence, we collected and screened a database (published data [33,43,45,47–50,65] and this paper) and eventually focused on 75 analyses of noble gas compositions in marine Fe-Mn crusts and nodules. In the $^{3}He/^{4}He$ versus $^{40}Ar/^{36}Ar$ and ^{4}He versus R/R_A bivariate diagrams (Figure 4), the different types of marine Fe-Mn precipitates differ significantly from each other, which is caused by the differences of the noble gases source and genetic mechanism of the crusts and nodules. In the metallogenetic processes of the Fe and Mn crusts and nodules, the $^{3}He/^{4}He$ ratio reveals decoupling of the ^{3}He and ^{4}He abundances, which ^{4}He abundance increases with the formation from hydrogenetic origin to diagenetic origin due to the effect of the radiogenic ^{4}He-rich sedimentary porewater or terrestrial sources and ^{3}He abundance increases with the input of IDPs or mantle sources. The diagenetic Fe-Mn nodules show the characteristics of high ^{3}He and ^{4}He abundances and high $^{3}He/^{4}He$ ratio. Compared with the Fe-Mn nodules, the seamount Fe-Mn crusts are mainly hydrogenetic origin [37], which makes the noble gases compositions of the crusts has the characteristics of multiple sources, showing a large range of $^{40}Ar/^{36}Ar$ ratio and a relative low $^{3}He/^{4}He$ ratio. Therefore, according to the genetic origin of the marine Fe-Mn precipitates, the formation of the SCS crusts/nodules were influenced by the growth conditions and the supply of metallogenic sources [62]. Thus, the characteristics of He and Ar isotope compositions of the SCS crusts/nodules resemble the properties of hydrogenetic Fe-Mn oxide/hydroxide precipitates, which reflects mainly the product of an equilibrium mixture between air-saturated seawater and radiogenic components.

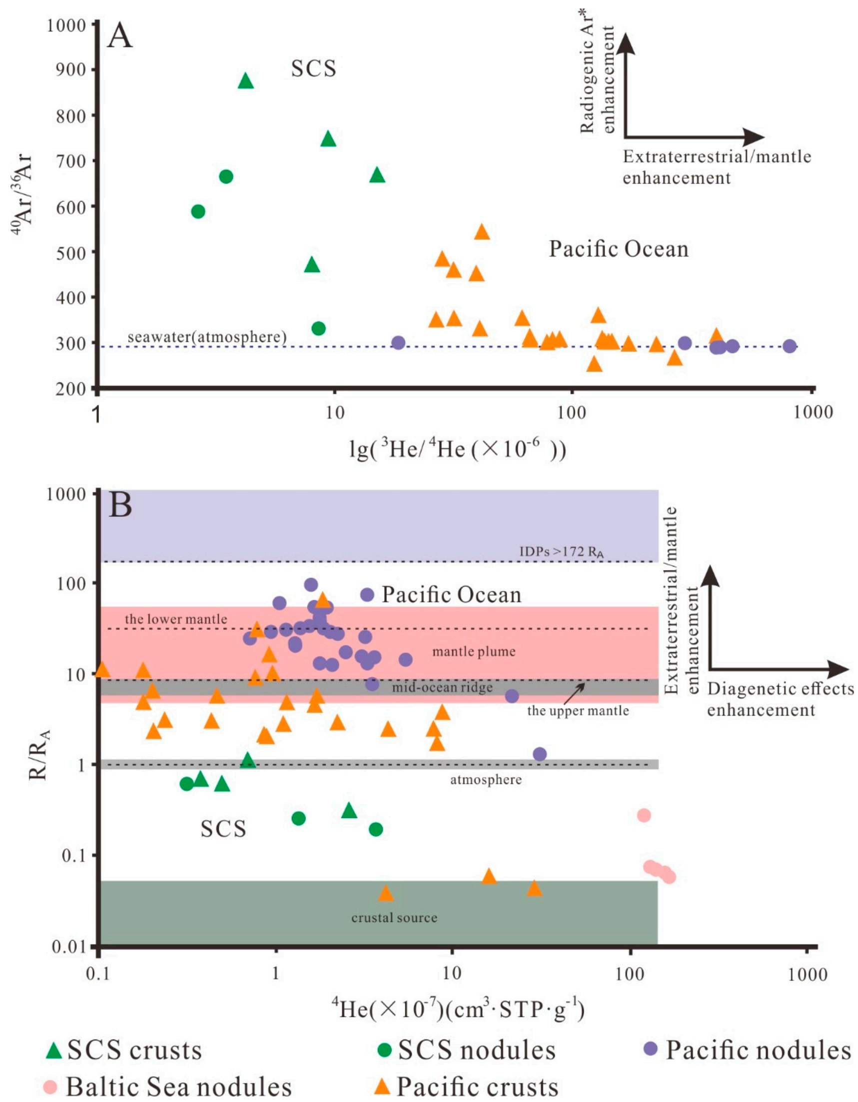

Figure 4. Plots of $^3He/^4He$ vs. $^{40}Ar/^{36}Ar$ (**A**) and ^4He concentration vs R/R_A (**B**) of Fe-Mn crusts and nodules from the South China Sea and Pacific Ocean (SCS crusts and nodules data from this study; Baltic Sea nodules data from [65]; Pacific nodules data from [33,43,45]; Pacific crusts data from [43,47–50]).

6. Conclusions

The ^3He concentrations and R/R_A values of the SCS crusts are generally higher than those of the SCS nodules, while ^4He and ^{40}Ar concentrations of the SCS crusts are lower than those of the SCS nodules. Both the SCS Fe-Mn crusts and nodules have lower ^3He contents and $^3He/^4He$ ratios than those of the Pacific Fe-Mn crusts and nodules, while the $^{40}Ar/^{36}Ar$ ratios of the SCS samples are significantly higher than those of the Pacific crusts and nodules. The relatively low $^3He/^4He$ ratios and high ^{40}Ar concentrations in the SCS samples were likely caused by the input of terrigenous detritus with high radiogenic ^4He and ^{40}Ar contents. The He and Ar were likely extracted from the SCS Fe-Mn crusts and nodules that their selves are the product of an equilibrium mixture between air-saturated seawater and radiogenic components during their growth history, while the excess ^3He in some SCS samples may represent minor mantle-derived origin.

Helium and Ar isotope compositions of Fe-Mn crusts and nodules show that there are different characteristics between the South China Sea and the Pacific Ocean due to their different sources and genetic processes. The characteristics of He and Ar isotope compositions of the SCS shallow-water crusts and nodules are similar to the properties of hydrogenetic Fe-Mn oxide/hydroxide precipitates, which reflects mainly the product of an equilibrium mixture between air-saturated seawater and radiogenic components.

Author Contributions: Y.G. and X.S. conceived the experiments. Y.G. analyzed the data and wrote this paper. Y.R. participated in the writing of this paper. X.S. substantially revised the manuscript. Z.X. and Z.G. pretreated the samples.

Funding: This work was funded by the 12th and 13th Five Year Plan Project of International Maritime Resources Investigation and Development (DY135-C1-1-06, DY125-13-R-05), National Nature Science Foundation of China (NSFC) (No. 40473024). The PhD Start-up Fund of Natural Science Foundation of Guangdong Province, China (2018A030310264), the open-funds of Key Laboratory of Marine Mineral Resources, Ministry of Land and Resources (KLMMR-2017-B-02) and Key Laboratory of Mineralogy and Metallogeny, Chinese Academy of Sciences (KLMM20170203).

Acknowledgments: We thank the Guangzhou Marine Geological Survey for supplying the samples and Wei Zhai and Four reviewers for their constructive comments. Laboratory analyses were supported by the Geological Analysis and Testing Center of the Beijing Research Institute of Uranium Geology, China National Nuclear Corporation.

Conflicts of Interest: The authors declare no conflict of interest.

References

1. Suess, H.E.; Wanke, H. On the possibility of a helium flux through the ocean floor. *Prog. Oceanogr.* **1965**, *3*, 347–353. [CrossRef]
2. Bieri, R.H.; Koide, M.; Goldberg, E.D. Noble gas contents of Pacific seawater. *J. Geophys. Res.* **1966**, *71*, 5243–5246. [CrossRef]
3. Clarke, W.B.; Beg, M.A.; Craig, H. Excess ^{3}He in the sea: Evidence for terrestrial primordial helium. *Earth Planet. Sci. Lett.* **1969**, *6*, 213–220. [CrossRef]
4. Jenkins, W.J.; Clarke, W.B. The distribution of ^{3}He in the Western Atlantic Ocean. *Deep-Sea Res. I* **1976**, *23*, 481–494. [CrossRef]
5. Craig, H.; Lupton, J.E. Helium-3 and mantle volatiles in the ocean and the oceanic crust. In *The Sea*; Emiliani, C., Ed.; John Wiley & Sons: New York, NY, USA, 1981; Volume 7, pp. 391–428.
6. Kaneoka, I.; Takaoka, N.; Clague, D.A. Noble gas systematics for coexisting glass and olivine crystals in basalt and dunite xenoliths from Loihi Seamount. *Earth Planet. Sci. Lett.* **1983**, *66*, 427–437. [CrossRef]
7. Lupton, J.E. A far-field hydrothermal plume from Loihi Seamount. *Science* **1996**, *272*, 976–979. [CrossRef] [PubMed]
8. Lupton, J.E. Hydrothermal helium plumes in the Pacific Ocean. *J. Geophys. Res.* **1998**, *103*, 15853–15868. [CrossRef]
9. Graham, D.W.; Humphris, S.E.; Jenkins, W.J.; Kurz, M.D. Helium isotope geochemistry of some volcanic rocks from Saint Helena. *Earth Planet. Sci. Lett.* **1992**, *110*, 121–131. [CrossRef]
10. Hilton, D.R.; Hammerschmidt, K.; Loock, G.; Friedrichsen, H. Helium and argon isotope systematics of the central Lau Basin and Valu Fa Ridge: Evidence of crust/mantle interactions in a back-arc basin. *Geochim. Cosmochim. Acta* **1993**, *57*, 2819–2841. [CrossRef]
11. Moreira, M.; Blusztajn, J.; Curtice, J.; Hart, S.; Dick, H.; Kurz, M.D. He and Ne isotopes in oceanic crust: Implications for noble gas recycling in the mantle. *Earth Planet. Sci. Lett.* **2003**, *216*, 635–643. [CrossRef]
12. Jenkins, W.J. Tritium and ^{3}He in the WOCE Pacific Programme. In *International WOCE Newsletter*; NOAA: Sliver Spring, MD, USA, 1996; Volume 23, pp. 6–8.
13. Schlosser, P.; Bonisch, G.; Rhein, M.; Bayer, R. Reduction of deep water formation in the Greenland Sea during the 1980s—Evidence from tracer data. *Science* **1991**, *251*, 1054–1056. [CrossRef] [PubMed]
14. Schlosser, P. Tritium/^{3}He dating of waters in natural system. In *Isotopes of Noble Gases as Tracers in Environmental Studies*; Intl Atom Energy Agency: Vienna, Austria, 1992; pp. 123–145.
15. Merrihue, C. Rare gas evidence for cosmic dust in modern Pacific red clay. *Ann. N. Y. Acad. Sci.* **1964**, *119*, 351–367. [CrossRef]
16. Ozima, M.; Takayanagi, M.; Zashu, S.; Amari, S. High ^{3}He/^{4}He ratios in ocean sediments. *Nature* **1984**, *311*, 449–451. [CrossRef]

17. Takayanagi, M.; Ozima, M. Temporal variation of $^{3}He/^{4}He$ ratio recorded in deep-sea sediment cores. *J. Geophys. Res.* **1987**, *92*, 12531–12538. [CrossRef]
18. Farley, K.A. Cenozoic variations in the flux of interplanetary dust recorded by ^{3}He in a deep-sea sediment. *Nature* **1995**, *376*, 153–156. [CrossRef]
19. Farley, K.A.; Patterson, D.B. A 100-kyr periodicity in the flux of extraterrestrial ^{3}He to the sea floor. *Nature* **1995**, *378*, 600–603.
20. Marcantonio, F.; Kumar, N.; Stute, M.; Anderson, R.F.; Seidl, M.A.; Schlosser, P.; Mix, A. A comparative study of accumulation rates derived by He and Th isotope analysis of marine sediments. *Earth Planet. Sci. Lett.* **1995**, *133*, 549–555. [CrossRef]
21. Marcantonio, F.; Anderson, R.F.; Stute, M.; Kumar, N.; Schlosser, P.; Mix, A. Extraterrestrial ^{3}He as a tracer of marine sediment transport and accumulation. *Nature* **1996**, *383*, 705–707. [CrossRef]
22. Marcantonio, F.; Higgins, S.; Anderson, R.F.; Stute, M.; Schlosser, P.; Rasbury, E.T. Terrigenous helium in deep-sea sediments. *Geochim. Cosmochim. Acta* **1998**, *62*, 1535–1543. [CrossRef]
23. Marcantonio, F.; Anderson, R.F.; Higgins, S.; Stute, M.; Schlosser, P.; Kubik, P. Sediment focusing in the central equatorial Pacific Ocean. *Paleoceanography* **2001**, *16*, 260–267. [CrossRef]
24. Matsuda, J.; Murota, M.; Nagao, K. He and Ne isotopic studies on the extraterrestrial material in deep-sea sediments. *J. Geophys. Res.* **1990**, *95*, 7111–7117. [CrossRef]
25. Nier, A.O.; Schlutter, D.J.; Brownlee, D.E. Helium and neon isotopes in deep Pacific Ocean sediments. *Geochim. Cosmochim. Acta* **1990**, *54*, 173–182. [CrossRef]
26. Nier, A.O.; Schlutter, D.J. Helium and neon in stratospheric particles. *Meteoritics* **1990**, *25*, 263–267. [CrossRef]
27. Nier, A.O.; Schlutter, D.J. The thermal history of interplanetary dust particles collected in earth's stratosphere. *Meteoritics* **1993**, *28*, 675–681. [CrossRef]
28. Tilles, D. Atmospheric noble gases from extraterrestrial dust. *Science* **1966**, *151*, 1015–1018. [CrossRef] [PubMed]
29. Tilles, D. Extraterrestrial excess ^{36}Ar and ^{38}Ar concentrations as possible accumulation-rate indicators for sea sediments. *Icarus* **1967**, *7*, 94–100. [CrossRef]
30. Amari, S.; Ozima, M. Extraterrestrial noble gases in deep-sea sediments. *Geochim. Cosmochim. Acta* **1988**, *52*, 1087–1095. [CrossRef]
31. Halbach, P.; Kriete, C.; Prause, B.; Puteanus, D. Mechanisms to explain the platinum concentration in ferromanganese seamount crusts. *Chem. Geol.* **1989**, *76*, 95–106. [CrossRef]
32. De Carlo, E.H.; McMurtry, G.M. Rare-earth element geochemistry of ferromanganese crusts from the Hawaiian Archipelago, central Pacific. *Chem. Geol.* **1992**, *95*, 235–250. [CrossRef]
33. He, G.W.; Sun, X.M.; Xue, T. *A Comparative Study of the Geology, Geochemistry and Metallogenetic Mechanism of Polymetallic Nodules and Cobalt-Rich Crusts from the Pacific Ocean*; Geological Publishing House: Beijing, China, 2011; pp. 39–45. (In Chinese)
34. Hein, J.R.; Koschinsky, A.; Bau, M.; Manheim, E.T.; Kang, J.K.; Roberts, L. Cobalt–rich ferromanganese crusts in the Pacific. In *Handbook of Marine Mineral Deposits*; CRC Press: Boca Raton, FL, USA, 2000; Chapter 9; pp. 239–279.
35. Hein, J.R.; Mizell, K.; Koschinsky, A.; Conrad, T.A. Deep-ocean mineral deposits as a source of critical metals for high- and green-technology applications: Comparison with land—Based resources. *Ore Geol. Rev.* **2013**, *51*, 1–14. [CrossRef]
36. Hein, J.R.; Conard, T.; Mizell, K.; Banakar, V.K.; Frey, F.A.; Sager, W.W. Controls on ferromanganese crust composition and reconnaissance resource potential, Ninetyeast Ridge, Indian Ocean. *Deep-Sea Res. I* **2016**, *110*, 1–19. [CrossRef]
37. Hein, J.R.; Koschinsky, A. Deep-ocean ferromanganese crusts and nodules. In *Treatise on Geochemistry*; Elsevier: Amsterdam, The Netherlands, 2014; pp. 273–291.
38. De Carlo, E.H. Paleoceanographic implications of rare earth element variability within a Fe-Mn crust from the central Pacific Ocean. *Mar. Geol.* **1991**, *98*, 449–467. [CrossRef]
39. Peucker-Ehrenbrink, B. Accretion of extraterrestrial matter during the last 80 million years and its effect on the marine osmium isotope record. *Geochim. Cosmochim. Acta* **1996**, *60*, 3187–3196. [CrossRef]
40. Klemm, V.; Levasseur, S.; Frank, M.; Hein, J.R.; Halliday, A.N. Osmium isotope stratigraphy of a marine ferromanganese crust. *Earth Planet. Sci. Lett.* **2005**, *238*, 42–48. [CrossRef]

41. Sano, Y.; Toyoda, K.; Wakita, H. He-3/He-4 ratios of marine ferromanganese nodules. *Nature* **1985**, *317*, 518–520. [CrossRef]
42. Boltenkov, B.S.; Kapitonov, I.N. Helium and Neon isotopes in abyssal oceanic nodules: Evidence of irregular growth of nodules. *Geochem. Int.* **1997**, *35*, 656–661.
43. Li, Y.H.; Li, J.C.; Song, H.B. A comparative study of helium isotope of polymetallic nodules and cobalt crusts. *Acta Geosci. Sin.* **1999**, *20*, 378–384. (In Chinese)
44. Li, Y.H.; Song, H.B.; Li, J.C. Extraterrestrial ^{3}He in marine polymetallic nodules: A potential method for measuring growth rate of nodules. *Sci. China Ser. B-Chem.* **2002**, *45*, 38–46. [CrossRef]
45. Bu, W.R.; Shi, X.F.; Zhang, M.J.; Liu, J.H. The sources of the noble gases in the oceanic Fe-Mn oxides: The evidences are from the helium isotopes in the polymetallic nodules from the Pacific C-C zone. *Acta Mineral. Sin.* **2011**, *31*, 684–685. (In Chinese)
46. Basu, S.; Stuart, F.M.; Klemm, V.; Korschinek, G.; Knie, K.; Hein, J.R. Helium isotopes in ferromanganese crusts from the central Pacific Ocean. *Geochim. Cosmochim. Acta* **2006**, *70*, 3996–4006. [CrossRef]
47. Sun, X.M.; Xue, T.; He, G.W.; Ye, X.R.; Zhang, M.; Lu, H.F.; Wang, S.W. Noble gas isotopic compositions of cobalt-rich ferromanganese crusts from the western Pacific Ocean and their geological implications. *Acta Geol. Sin.* **2007**, *81*, 90–98.
48. Bu, W.R.; Shi, X.F.; Zhang, M.J.; Liu, J.H.; Glasby, G.P. He, Ne and Ar isotopic composition of Fe-Mn crusts from the western and central Pacific Ocean and implications for their genesis. *Sci. China Ser. D-Earth Sci.* **2007**, *50*, 857–868. [CrossRef]
49. Ye, X.R.; Fang, N.Q.; Ding, L.; Zhang, M.J. The noble gas contents and helium and argon isotopic compositions in the cobalt–rich crusts from the Magellan Seamounts. *Acta Petrol. Sin.* **2008**, *24*, 185–192. (In Chinese)
50. Li, J.S.; Fang, N.Q.; Shi, X.F.; Ren, X.W.; Liu, J.H.; Cui, Y.C. Helium and argon isotopic compositions of various crustal layers of a Co-rich Fe-Mn crust from central Pacific. *Earth Sci. J. China Univ. Geosci.* **2012**, *37*, 93–100. (In Chinese)
51. Wang, S.H.; Yan, W.; Song, H.B. Mapping the thickness of the gas hydrate stability zone in the South China Sea. *Terr. Atmos. Ocean. Sci.* **2006**, *17*, 815–828. [CrossRef]
52. Zhou, D.; Yao, B.C. Tectonics and sedimentary basins of the South China Sea: Challenges and progresses. *J. Earth Sci.* **2009**, *20*, 1–12. [CrossRef]
53. Zhao, F.; Alves, T.M.; Wu, S.G.; Li, W.; Huuse, M.; Mi, L.J.; Sun, Q.L.; Ma, B.J. Prolonged post-rift magmatism on highly extended crust of divergent continental margins (Baiyun Sag, South China Sea). *Earth Planet. Sci. Lett.* **2016**, *445*, 79–91. [CrossRef]
54. Winsner, M.G.; Wang, Y.B.; Zheng, L.F. Fallout of volcanic ash to the deep South China Sea induced by the 1991 eruption of Mount Pinatubo. *Geology* **1995**, *23*, 885–888. [CrossRef]
55. Haeckel, M.; Beusekom, J.V.; Wiesner, M.G.; König, I. The impact of the 1991 Mount Pinatubo tephra fallout on the geochemical environment of the deep sea sediments in the South China Sea. *Earth Planet. Sci. Lett.* **2001**, *193*, 151–166. [CrossRef]
56. Xia, S.H.; Zhao, D.P.; Sun, J.L.; Huang, H.B. Teleseismic imaging of the mantle beneath southernmost China: New insights into the Hainan plume. *Gondwana Res.* **2016**, *36*, 46–56. [CrossRef]
57. Zhang, W.Y.; Zhang, F.Y.; Chen, R.H.; Zhang, X.Y. Constituents of matter and sedimentation fluxes and sedimentation rates of deep-water sedimentation during the Late Pleistocene in the South China Sea. *Acta Sedimentol. Sin.* **2002**, *20*, 668–674. (In Chinese)
58. Knnett, P. *Marine*; Prentice-Hall, Inc.: Englewood Cliffs, NJ, USA, 1982.
59. Huang, W.; Wang, P.X. Sediment mass and distribution in the South China Sea since the Oligocene. *Sci. China Ser. D-Earth Sci.* **2006**, *49*, 1147–1155. [CrossRef]
60. Yang, S.X.; Qiu, Y.; Zhu, B.Y. *Atlas of Geology and Geophysics of the South China Sea*; China Navigation Publications: Tianjin, China, 2015.
61. Guan, Y.; Sun, X.M.; Ren, Y.Z.; Jiang, X.D. Mineralogy, geochemistry and genesis of the polymetallic crusts and nodules from the South China Sea. *Ore Geol. Rev.* **2017**, *89*, 206–227. [CrossRef]
62. Guan, Y.; Sun, X.M.; Shi, G.Y.; Jiang, X.D.; Lu, H.F. Rare earth elements (REE) composition and constraints on the genesis of the polymetallic crusts and nodules in the South China Sea. *Acta Geol. Sin.* **2017**, *91*, 1757–1766. [CrossRef]

63. Bau, M.; Schmidt, K.; Koschinsky, A.; Hein, J.; Kuhn, T.; Usui, A. Discriminating between different genetic types of marine ferromanganese crusts and nodules based on rare earth elements and yttrium. *Chem. Geol.* **2014**, *381*, 1–9. [CrossRef]
64. Huh, C.A.; Ku, T.L. Radiochemical observations on manganese nodules from three sedimentary environments in the north Pacific. *Geochim. Cosmochim. Acta* **1984**, *48*, 951–963.
65. Anufriev, G.S.; Boltenkov, B.S. Ferromanganese nodules of the Baltic Sea: Composition, helium isotopes, and growth rate. *Lithol. Miner. Resour.* **2007**, *42*, 240–245. [CrossRef]
66. Faure, G. *Principles of Isotope Geology*, 2nd ed.; John Wiley & Sons: New York, NY, USA, 1986; pp. 66–92.
67. Jaffer, A.H.; Flynn, K.F.; Glendemin, L.E.; Bentley, W.T.; Essling, A.M. Precision measurement of the half-lives and specific activities of ^{235}U and ^{238}U. *Phys. Rev. C* **1971**, *4*, 1889–1907. [CrossRef]
68. Zhai, W.; Sun, X.M.; Wu, Y.S.; Sun, Y.Y.; Hua, R.M.; Ye, X.R. He-Ar isotope geochemistry of the Yaoling-Meiziwo tungsten deposit, north Guangdong Province: Constraints on Yanshanian crust–mantle interaction and metallogenesis in SE China. *Chin. Sci. Bull.* **2012**, *57*, 1150–1159. [CrossRef]
69. Stuart, F.M.; Lee, M.R. Micrometeorites and extraterrestrial He in a ferromanganese crust from the Pacific Ocean. *Chem. Geol.* **2012**, *322*, 209–214. [CrossRef]
70. Nier, A.O.; Schlutter, D.J. Extraction of helium from individual interplanetary dust particles by step-heating. *Meteoritics* **1992**, *27*, 166–173. [CrossRef]
71. Pepin, R.O.; Plama, R.L.; Schlutter, D.J. Noble gases in interplanetary dust particles, I. The excess of helium-3 problem and estimates of the relative fluxes of solar wind and solar energetic particles in interplanetary space. *Meteorit. Planet. Sci.* **2000**, *35*, 495–504. [CrossRef]
72. Marty, B.; Robert, P.; Zimmermann, L. Nitrogen and noble gases in micrometeorites. *Meteorit. Planet. Sci.* **2005**, *40*, 881–894. [CrossRef]
73. Burnard, P.G.; Hu, R.Z.; Turner, G.; Bi, X.W. Mantle, crustal and atmospheric noble gases in Ailaoshan gold deposits, Yunnan Province, China. *Geochim. Cosmochim. Acta* **1999**, *63*, 1595–1604. [CrossRef]
74. Schlosser, P.; Winckler, G. Noble gases in the ocean and ocean floor. Noble Gases in Geochemistry and Cosmochemistry. *Rev. Mineral. Geochem.* **2002**, *47*, 701–730. [CrossRef]
75. Ozima, M.; Podosek, F.A. *Noble Gas Geochemistry*; Cambridge University Press: London, UK, 2001; 367p.
76. Takahata, N.; Watanabe, T.; Shirai, K.; Nishizawa, M.; Sano, Y. Helium isotopes of seawater in adjacent sea of Nansei Islands, southwest Japan. *Geochem. J.* **2004**, *38*, 593–600. [CrossRef]
77. Sano, Y.; Takahata, N.; Gamo, T. Helium isotopes in South Pacific deep seawater. *Geochem. J.* **1995**, *29*, 377–384. [CrossRef]
78. Weiss, R.F. Solubility of helium and neon in water and seawater. *J. Chem. Eng. Data* **1971**, *16*, 235–241. [CrossRef]
79. Ballentine, C.J.; Burgess, R.; Marty, B. Tracing fluid origin, transport and interaction in the crust. *Rev. Mineral. Geochem.* **2002**, *47*, 539–614. [CrossRef]
80. Craig, H.; Clarke, W.B.; Beg, M.A. Excess ^{3}He in deep water on the East Pacific Rise. *Earth Planet. Sci. Lett.* **1975**, *26*, 125–132. [CrossRef]
81. Lupton, J.E.; Craig, H. A major helium–3 source at 15° S on the East Pacific Rise. *Science* **1981**, *214*, 13–18. [CrossRef] [PubMed]
82. Takahata, N.; Tokukake, T.; Shirai, K.; Fujio, S.; Tanaka, K.; Sano, Y. Helium isotopes of seawater in the Philippine Sea and the western North Pacific. *Geochem. J.* **2010**, *44*, 451–460. [CrossRef]
83. Sano, Y.; Kosugi, T.; Takahata, N.; Yokochi, R. Helium isotopes in Pacific waters from adjacent region of Honshu, Japan. *J. Oceanogr.* **2004**, *60*, 625–630. [CrossRef]
84. Ballentine, C.J.; Burnard, P.G. Production, release and transport of noble gases in the continental crust. *Rev. Mineral. Geochem.* **2002**, *47*, 481–538. [CrossRef]
85. Poreda, R.J.; Jenden, P.D.; Kaplan, I.R.; Craig, H. Mantle helium in Sacranmento basin natural gas Wells. *Geochim. Cosmochim. Acta* **1986**, *50*, 2847–2853. [CrossRef]
86. Oxburgh, E.R.; O'nions, R.K.; Hill, R.I. Helium isotopes in sedimentary basin. *Nature* **1986**, *324*, 632–635. [CrossRef]
87. Oxburgh, E.R.; O'nions, R.K. Helium loss, tectonics, and the terrestrial heat budget. *Science* **1987**, *237*, 1583–1588. [CrossRef] [PubMed]
88. Aplin, A.C.; Cronan, D.S. Ferromanganese oxide deposits from the central Pacific Ocean, II. Nodules and associated sediments. *Geochim. Cosmochim. Acta* **1985**, *49*, 437–451. [CrossRef]

89. Halbach, P.; Hebisch, U.; Scherhag, C. Geochemical variations of ferromanganese nodules and crusts from different provinces of the Pacific Ocean and their genetic control. *Chem. Geol.* **1981**, *34*, 3–17. [CrossRef]
90. Hein, J.R.; Conrad, T.A.; Dunham, R.E. Seamount characteristics and minesite model applied to exploration-and mining-lease-block selection for Cobalt-rich ferromanganese crusts. *Mar. Georesour. Geotechnol.* **2009**, *27*, 160–176. [CrossRef]
91. Konstantinova, N.; Cherkashov, G.; Hein, J.R.; Jose, M.; Luis, D.; Pedro, M.; Vladislav, K.; Fedor, M. Composition and characteristics of the ferromanganese crusts from the western Arctic Ocean. *Ore Geol. Rev.* **2016**, *87*, 88–99. [CrossRef]
92. Muinos, S.B.; Hein, J.R.; Frank, M.; Monteiro, J.H.; Gaspar, L.; Conrad, T.; Pereira, H.G.; Abrantes, F. Deep-sea Fe-Mn crusts from the Northeast Atlantic Ocean: Composition and Resource Considerations. *Mar. Georesour. Geotechnol.* **2013**, *31*, 40–70. [CrossRef]
93. Rajani, R.P.; Banakar, V.K.; Parthiban, G.; Mudholkar, A.V.; Chodankar, A.R. Compositional variation and genesis of ferromanganese crust of the Afanasiy-Nikitin Seamount, Equatorial Indian Ocean. *J. Earth Syst. Sci.* **2005**, *114*, 51–61. [CrossRef]
94. Bonatti, E.; Kraemer, T.; Rydell, H. Classification and genesis of submarine iron-manganese deposits. In *Ferromanganese Deposits on the Ocean Floor*; Horn, D.R., Ed.; National Science Foundation: Washington, DC, USA, 1972; pp. 149–166.